MODELING SHORT-PERIOD SURFACE WAVES FROM SMALL EXPLOSIONS AT THE SHAGAN TEST SITE

Jessie L. Bonner,[1] Jeffrey L. Orrey,[2] and Anca C. Rosca[1]

Weston Geophysical Corporation,[1] GeoVisual Technologies Inc.[2]

Sponsored by the National Nuclear Security Administration
Office of Nonproliferation Research and Engineering
Office of Defense Nuclear Nonproliferation

Contract No. DE-FG02-00ER83123

ABSTRACT

The objective of our research is to study the generation and propagation of short-period (0.2 to 12 secs) surface waves from a variety of different classifications of explosions. Thus, we have assembled a dataset of local and regional recordings of single-fired chemical explosions (Non-Proliferation Experiment and Balapan Depth of Burial shots), coal-mining explosions (including cast and coal shots from northern Arizona), rock fragmentation shots (Arizona), and quarry blasts (Central Texas). The dataset includes detailed source parameters including origin times, shot patterns, and additional information key to modeling the physics of the various explosions. In the upcoming year, we plan to supplement this dataset with additional close-in and regional recordings of hard-rock fragmentation blasts in Minnesota.

During the past year, our research has focused on the near-source modeling of twelve single-fired chemical explosions detonated in boreholes at the former Soviet nuclear test site near the Shagan River (STS) in Kazakhstan. The depths of these explosions ranged from 2.5 to 550 m, while the explosive yield varied from 2 to 25 tons. To quantify the generation and propagation of *Rg* from these explosions, we developed a shallow velocity model for STS by combining surficial and borehole geology with velocity profiles from Bonner *et al*. (2001). This model divides the region into several zones, including a fast southwestern (SW) section and a slow northeastern (NE) section separated by transitional regions. We then determined the attenuation quality factor for *Rg* (Q_{Rg}) at frequencies of 0.5, 1, 1.8, 3.5, and 5.5 Hz. In the slower NE section, *Rg* is strongly attenuated and has a Q_{Rg} value of approximately 10 at 1 Hz that increases with increasing frequency. However, for paths within the faster SW section, we observe Q_{Rg} values that are on average 5 times greater and as large as an order of magnitude greater. These differences in velocity and attenuation may be the source of spatial biases in regional and teleseismic waveform characteristics observed at STS (Ringdahl *et al*., 1992; Phillips *et al*., 2001). We have ported a numerical wave field modeling method, the Generalized Fourier Method (GFM) developed by Orrey *et al.* (2002), to a Linux computer cluster in order to generate Green's functions for the 3D STS model. Our preliminary results suggest that the modeling will provide accurate characterizations of propagation effects at STS. Strong lateral velocity and attenuation variations at STS affect the propagation of short period surface waves. We have also used the method to examine near-source conversion of *Rg* into *S* phases. For the next stage of this research, we propose to combine the MineSeis code of Yang (1998) with the GFM code to model delay-fired mining explosions in complex near-source and regional 3D media.

OBJECTIVES

The objectives of this research project are to create physically realistic models of short-period (0.2 to 12 seconds) surface wave generation from small chemical explosions and different classifications of mine blasts, and to understand the propagation characteristics of these surface waves, including the scattering of *Rg* into *Lg,* in complex tectonic regimes. To accomplish these objectives, we have:

- Collected local and regional seismic data sets with short-period (0.5 to 12 sec) surface waves generated from chemical and mining explosions in North America, India, and Kazakhstan,
- Initiated use of a numerical modeling package to generate short-period surface waves from different explosion sources and to propagate them through complex, 3D media, and
- Compared preliminary numerical results to empirical data to aid in development of regional explosion discriminants based upon surface waves.

The progress in the development of the 3D surface wave modeling program and the preliminary results of applying the technique to a model for the Shagan Test Site (STS) in Kazakhstan are discussed in this paper.

RESEARCH ACCOMPLISHED

Regional Wavefield Modeling in 3D Media Using the Generalized Fourier Method

We are applying a numerical wavefield modeling method to generate Green's functions for regional, 3D Earth models. Numerical methods allow the incorporation of realistic structural features such as strong lateral velocity variations, anelastic attenuation and surface topography, which affect the propagation of short period surface waves. However, numerical methods such as finite difference or pseudospectral are computationally very expensive in 3D, where doubling the frequency of a simulation requires eight times as many nodes for a fixed spatial sampling of the wave field. For a particular method, the overall computational effort increases by roughly an order of magnitude with a doubling of frequency (Orrey, 1995).

The numerical method we use is a generalization of the Fourier pseudospectral method. In the Fourier pseudospectral approximation, the spatial approximations of the field variables are truncated Fourier series. Derivatives in the equations of motion are computed by performing spatial FFTs, multiplying by wave numbers, and performing inverse FFTs. The overall efficiency of the Fourier method using second-order time integration is higher for 3D elastic applications compared to a fourth-order in space, second-order in time finite difference method when measured in terms of CPU and memory requirements (Fornberg, 1987). The principal disadvantage of the standard Fourier method, particularly for our applications to surface wave scattering mechanisms, is that boundary conditions at grid edges are intrinsically periodic due to the implementation with FFTs. Therefore, standard Fourier solutions involving interactions of the wave field with the traction-free surface of the earth are inherently flawed. In the Generalized Fourier Method (GFM) used for our simulations, this periodicity is removed for the free surface by supplementing the trigonometric basis functions of the standard method with additional, discontinuity functions that approximate the spatial discontinuities of the field variables at the free surface. For a detailed discussion of the GFM method, the reader is referred to Orrey *et al*. (2002).

An additional advantage of the Fourier method over finite differencing is that the FFT computations allow for efficient solution on parallel computer architectures (Orrey and Robinson, 2002; Furumura *et al.,* 1998), with individual processors computing FFTs for separate columns and rows in the 3D computational grid. In our present implementation of GFM on a nine-node Linux cluster, the computational grid is partitioned into planar sections and distributed among processors as shown in Figure 1, using the Message Passing Interface for parallelization. During each time iteration of wave field evolution, horizontal sections of the computational grid are initially distributed over the NP processing elements, with NZ/NP node planes passed to each processor. After computing the X and Y differentials of the equations of motion via FFTs along rows and columns of each plane, the data set is transposed to

the distribution shown on the right hand side of Figure 1 for computation of differentials in Z. This step requires significant interprocessor communication. The data set is then transposed back to the distribution on the left hand side of Figure 1 for the next time iteration. The code has been optimized for data transfer, interprocessor communication and processor latency, with profiling tools used to tune the parallel performance.

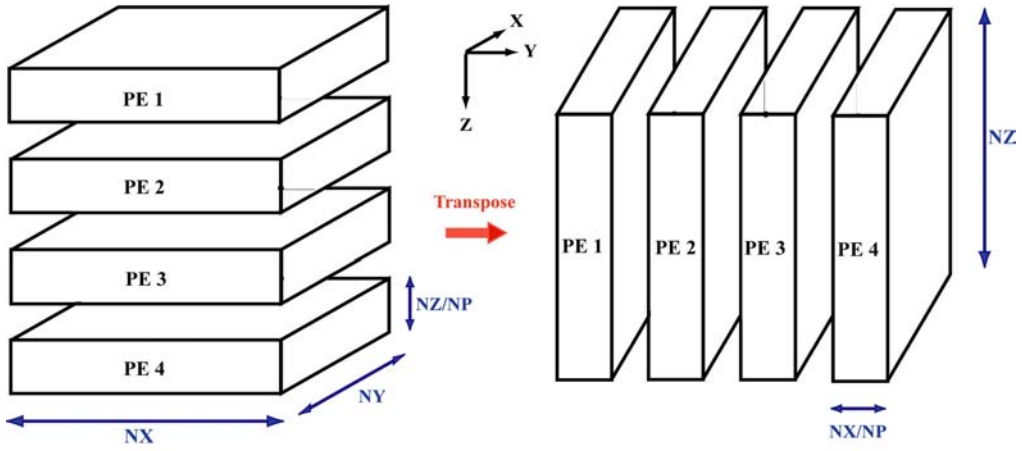

Figure 1. Schematic of domain partitioning for a four-processor distribution of the computational grid and the transpose operation requiring interprocessor communication.

Modeling *Rg* Generation and Propagation at the Shagan Test Site

We have modeled the *Rg* generation and propagation from single-fired explosions at the former Soviet Union Test Site near the Shagan River in Balapan, Kazakhstan. These explosions were conducted to destroy the unused boreholes as part of the decommissioning of the facility. The first set of explosions were conducted in boreholes 1071, 1311, 1381, and 1349 with explosive weights of 25 tons and emplacement depths of 28 m, 50 m, 300 m, and 550 m, respectively. The explosives were emplaced in neogenic clays (1311) and crystalline rock (1071, 1349 and 1381). The primary scientific objective of this series of explosions was to determine the effect of depth of burial (DOB) on the discrimination of nuclear explosions. In addition to the DOB study, six additional explosive borehole closures were recorded, and the depth of the explosives emplacement for these closures ranged from 2.5 to 46 meters with 2 ton yields. The charge in borehole 1381 was detonated in granoseyenites, while the charges in five other boreholes (1327, 1386, 1389, 1409 and 1419) were detonated in neogenic clays. In the following paragraphs, we describe the development of the velocity and attenuation models for STS and present the preliminary results of modeling the observed data with the GFM3D technique.

Variations in STS geology were first noted when we inverted the short-period Rayleigh waves for shallow velocity structure (Bonner *et al.*, 2001). We generated dispersion curves for the station-source pairs for all 10 explosions and found that the test site comprises several distinct regions separated by transitional zones. The group velocity tomography map for 1 Hz *Rg* showed a relatively high velocity region to the southwest (SW) and a low velocity region in the northeast (NE) separated by transition zones. These regions of the test site correlate with zones determined from differences in teleseismic magnitudes (Ringdal *et al*., 1992). We suspect the faster velocities in the SW region are related to crystalline rocks at or near the surface. Cores for test hole 1383 show crystalline rocks within 5 m of the surface. The low velocities associated with the transition zone follow the Shagan River towards the southwest, and may be related to alluvium overlying the intrusive crystalline rocks near this section of the test site. Lithologic logs from boreholes in this region confirm that alluvium and weathered rock with thickness as great as 350 m overlie the crystalline rocks. In the NE region logs show thick sections of alluvium and unconsolidated tuffs that overlie the Paleozoic sedimentary section. We inverted the dispersion curves for the paths in the SW and

NE sections of STS and determined five distinct velocity profiles for this region (Figure 2). We then used these velocity profiles to develop an initial 3D *P*- and *S*-wave velocity model for STS (Figure 3). We note that over the coming months, we plan to increase the complexity of the 3D model, however the preliminary model is adequate for initial numerical simulations.

The model was developed using a 2 x 2 x 0.125 km spatial discretization (hence the blocky shape of the model as shown in Figure 3), and then resampled to 0.125 x 0.125 x 0.125 km. This discretization resulted in 243 grid points (30.4 km) in both the East-West and North-South directions and 63 grid points (7.8 km) in the vertical direction for a total of 3.7 million nodes. The discretization is designed so that the smallest wavelength (λ) surface wave (in our case, 4 Hz *Rg* with λ~ 0.5 km) is sampled by at least four grid nodes. The parameters for the GFM runs are listed in Table 1. The computer time necessary to run a model with these dimensions in order to synthesize 15 seconds of data is approximately 6 hours using a nine-node Linux cluster. This computational performance was obtained for models that do not incorporate anelasticity. Once we have incorporated anelasticity into the parallel implementation of the code, using the method of Emmerich and Korn (1987), the performance is expected to decrease by about 20% due to the additional computational requirements. However, we are working to implement additional optimization features and expect to keep the run times within a practical time frame for the frequency and distance ranges of interest.

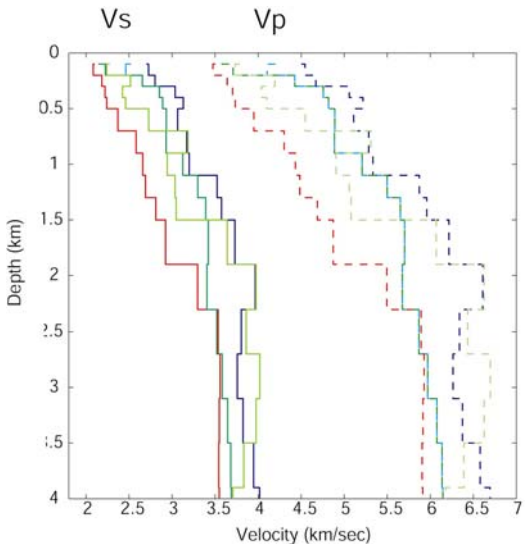

Figure 2. *P*- and *S*-wave velocity profiles used to develop a 3D model for the STS.

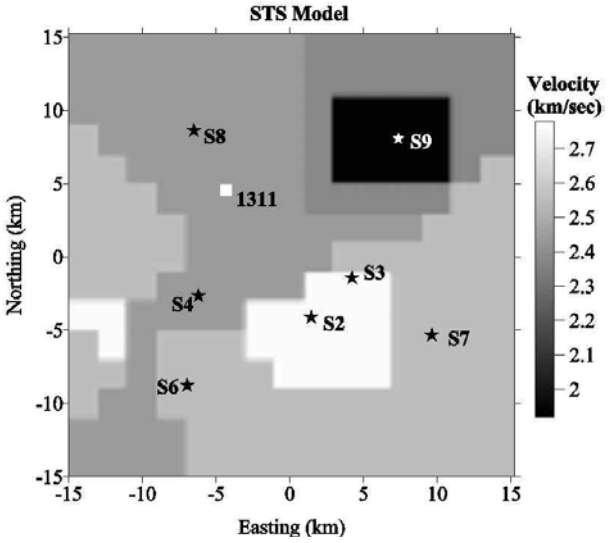

Figure 3. Shear-wave velocity at 0.2 km depth for the STS. Also shown are the location of borehole 1311 and stations that recorded this explosive borehole closure.

Table 1. STS 3D Modeling Parameters

Parameter	Value	Parameter	Value
Spatial discretization	0.125 km	E-W extent of model	30.4 km
Temporal discretization	0.0112 sec	N-S extent of model	30.4 km
Number of E-W grid points	243	Vertical extent of model	7.8 km
Number of N-S grid points	243	Number of time steps	4016
Numbr of Vertical grid points	63	Simulation time	15 sec

We modeled the local amplitude decay (Figure 4) for the explosions based upon the location of the travel paths relative to the SW and NE sections of STS. Our initial modeling of *Rg* attenuation considered all data and determined similar Q values (Q_{Rg} ~ 10 at 1 Hz) as Meyers *et al.*, (1999) who at that time were only able to examine the data from three explosions. We analyzed the data from all ten explosions conducted during these experiments. We searched for station pairs with similar source-to-station azimuths and found two such paths for the slow velocity NE section of the test site, 3 paths in the faster SW section, and one path that consisted of approximately 50% of each section. We computed the Q_{Rg} using the following equation (Aki and Richards, 1980) which includes geometric spreading and analastic attenuation;

$$A_{Rg} \propto \frac{Ao}{\sqrt{r}} \exp\left(\frac{-wr}{2C_{Rg}(w)Q(w)}\right)$$

where A_{Rg} is the *Rg* amplitude at distance *r* and angular frequency w, C_{Rg} is the *Rg* velocity determined from dispersion curves, Q is the quality factor, and Ao controls the overall amplitude level. We calculated the Q_{Rg} at frequencies of 0.5, 1, 1.8, 3.5, and 5.5 Hz and the results are shown in Figure 4. *Rg* is strongly attenuated in the slower NE section and has a value of approximately 10 at 1 Hz that increases with increasing frequency. However, for paths within the faster SW section, we see Q values that are on average 5 times greater and are as large as an order of magnitude greater. For each section we incorporated the mean value at 1 Hz into a Q model for the upper crust of STS; however, the initial simulations presented in this paper were completed without anelasticity; anelasticity is currently being incorporated into the parallel version of the GFM3D code.

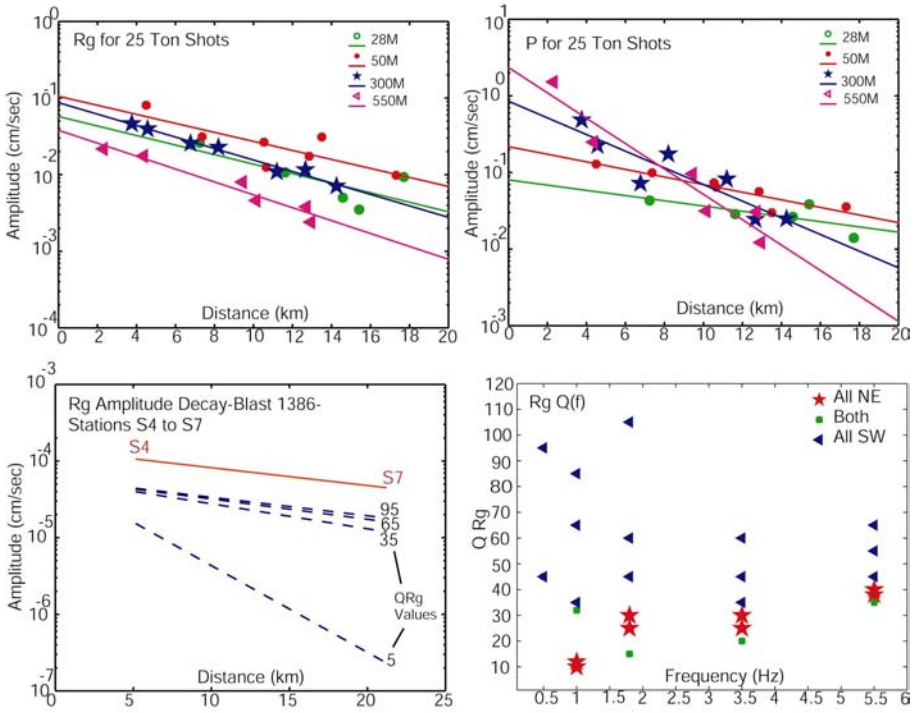

Figure 4. (Top Left) Amplitude decay of *Rg* for the 25 ton shots at STS approximated with a least squares line for each depth. Note that the shallowest explosion had reduced *Rg* amplitudes equivalent to the 300 m shot. Given that the P wave amplitudes are also smaller (Top Right), the explosives may have not detonated full yield, however, differences in source mechanics can not be ruled out. (Lower Left), 1 Hz Rg amplitude decay between stations S4 and S7 for the explosion at Hole 1386 (See Figure 5). The solid red line connects the observed data points, while the dashed lines are the calculated decay based upon Q values of 5, 35, 65, and 95. The scatter in the amplitude decay can be reduced by considering propagation in the NE and SW sections separately. We note very high attenuation (low Q; Lower Right) in the NE section with lower attenuation in the SW section.

The long-term goal of this modeling project is to quantify the near-source processes, such as secondary source effects (e.g., scattering, spall, block motions, tectonic release), that affect regional seismograms recorded in different tectonic regimes. The first steps of the project, completed for this paper, are 1) testing the accuracy of the GFM3D method in modeling local data that has traversed paths of simple and/or complex geologies and 2) performing initial analyses of the effects of small-scale heterogeneities on *Rg* generation and propagation. To accomplish the first goal, we completed GFM3D simulations for three different sources in the STS 3D velocity model. A point source explosion was considered for the source and placed at the locations and depths of three of the DOB experiment boreholes (Table 2). We have not modeled the data for a fourth DOB explosion detonated at 28 meters in borehole 1071; however, we plan to model this explosion together with six other explosions in the region during the upcoming year.

Table 2. Source Locations for GFM3D Simulations.

Borehole	Latitude	Longitude	Yield (tons)	Depth (m)	Model X	Model Y
1311	49.9412	78.7860	25	50	-4.58	4.53
1381	49.8837	78.8147	25	300	-2.53	-1.87
1349	49.8794	78.8493	25	550	-0.05	-2.35

The results of performing the GFM3D simulations on the preliminary STS model are shown in Figures 5-7. Figure 5 presents the comparison of the observed and modeled data in different bandwidths for station S2 from the 25-ton explosion detonated at 50 m depth in borehole 1311. The synthetic seismograms are shown as the first three traces (in order N, E, and Z) in Figures 6 and 7 and are compared with the three-component recordings (last three traces in order N, E, and Z) from a seven station local network deployed by Los Alamos National Laboratory. The observed and synthetic traces were converted to displacement, band-pass filtered between 0.5 and 4 Hz, plotted on equivalent time scales, and normalized to the maximum amplitude in each trace.

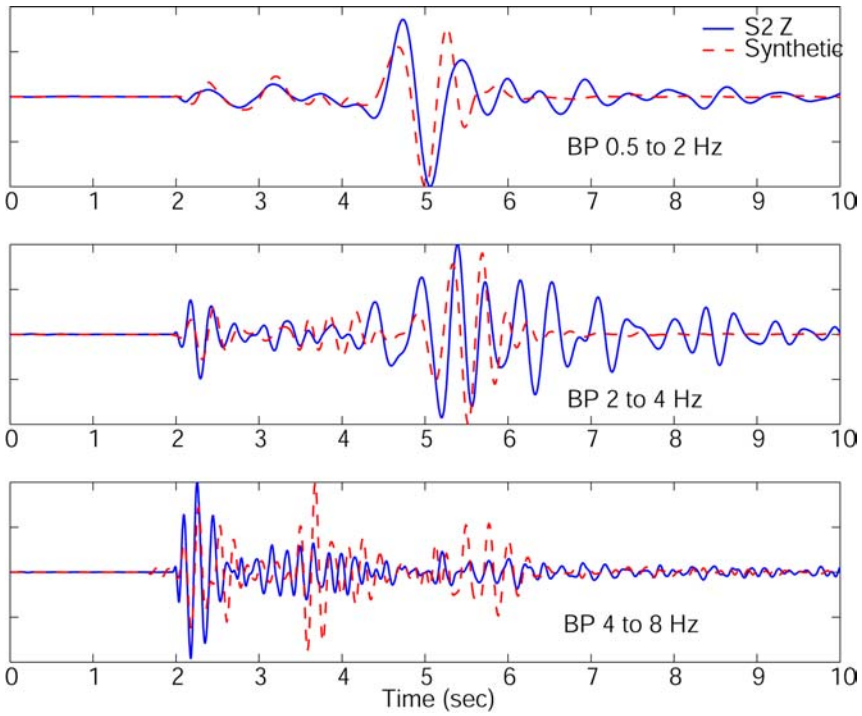

Figure 5. Comparison of station S2 data for the explosion at Borehole 1311 with GFM3D simulations band-passed at (top) 0.5 to 2 Hz, (middle) 2 to 4 Hz, and (bottom) 4 to 8 Hz.

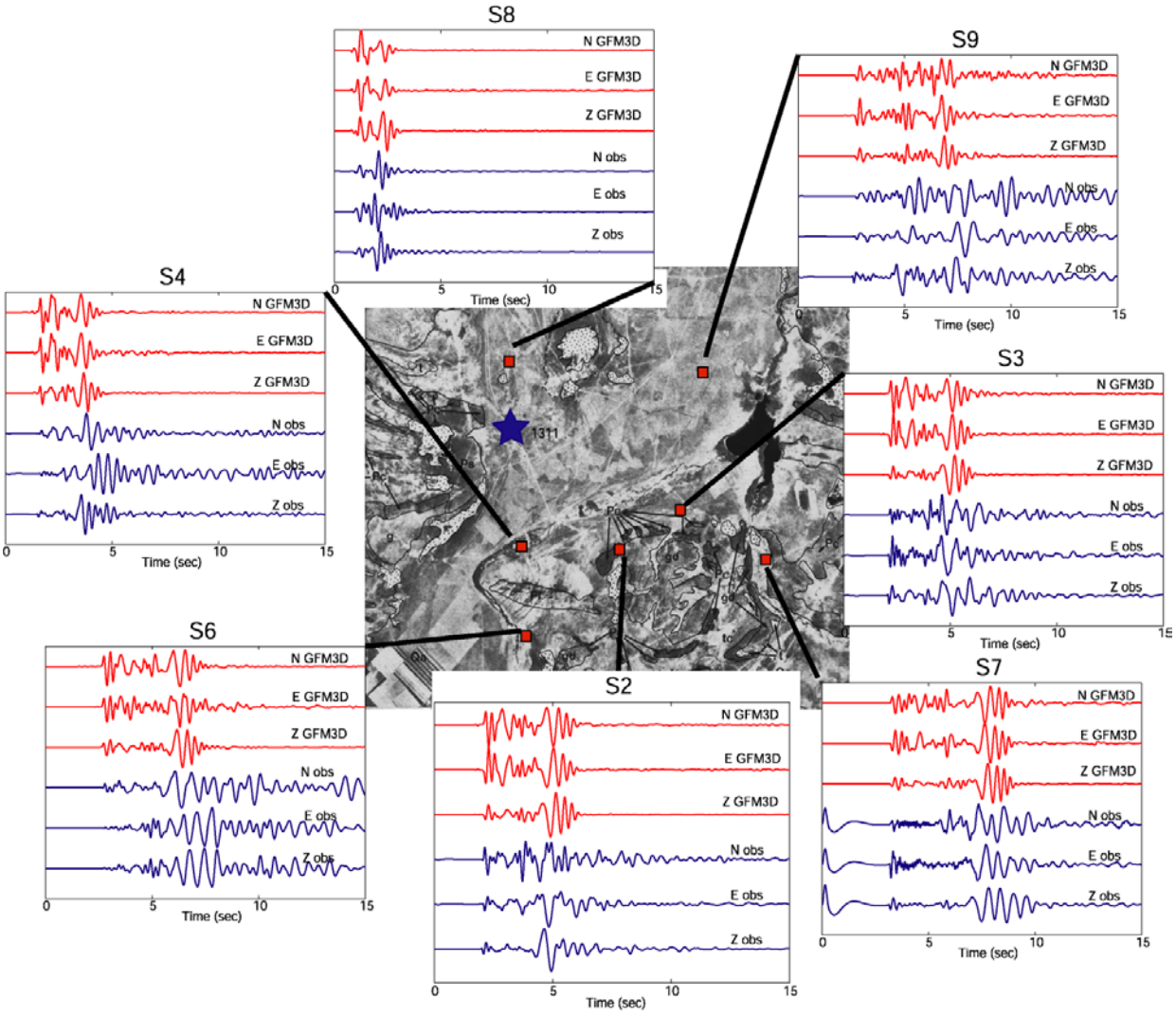

Figure 6. Comparison of observed local seismograms from the explosion at borehole 1311 with GFM3D synthetic traces. Each subplot corresponds to a station that recorded this 50-ton explosion at a depth of 50 m. The first three traces are the N, E, and Z traces synthesized using the STS velocity model and the GFM3D code followed by the observed N, E, and Z waveforms. All data were filtered between 0.5 and 4 Hz. The overhead imagery and interpreted geology is from Davis and Berlin (1992).

Based on the initial STS model, our results are very promising, as the simulated traces show good correlation (in both the arrival times and the waveform characteristics of the *P*, S, and *Rg* arrivals) to the observed data for most of the stations. The largest observed arrival at all seven stations is *Rg*, however, the complexity of the *Rg* packet varies significantly at each station. For example, the observed data at station S8 shows a high frequency, pulse-like Rayleigh wave with relatively no dispersion as compared to station S7 that shows longer period, dispersed *Rg*. We were able to simulate the approximate *Rg/P* ratios observed at 5 of 7 stations, with the modeled data for stations near the source (S4 and S8) predicting larger *P* wave arrivals than observed. For most of the stations, the modeling predicted short-period Rayleigh wave trains that replicated significant portions of the observed *Rg*. At stations S3, S4, and S7, the modeled *Rg* (Z components) and the observed data have high correlation throughout the entire wave packet. At other stations (S2, S6, and S8), the model traces only match the initial cycles of the *Rg* wave train.

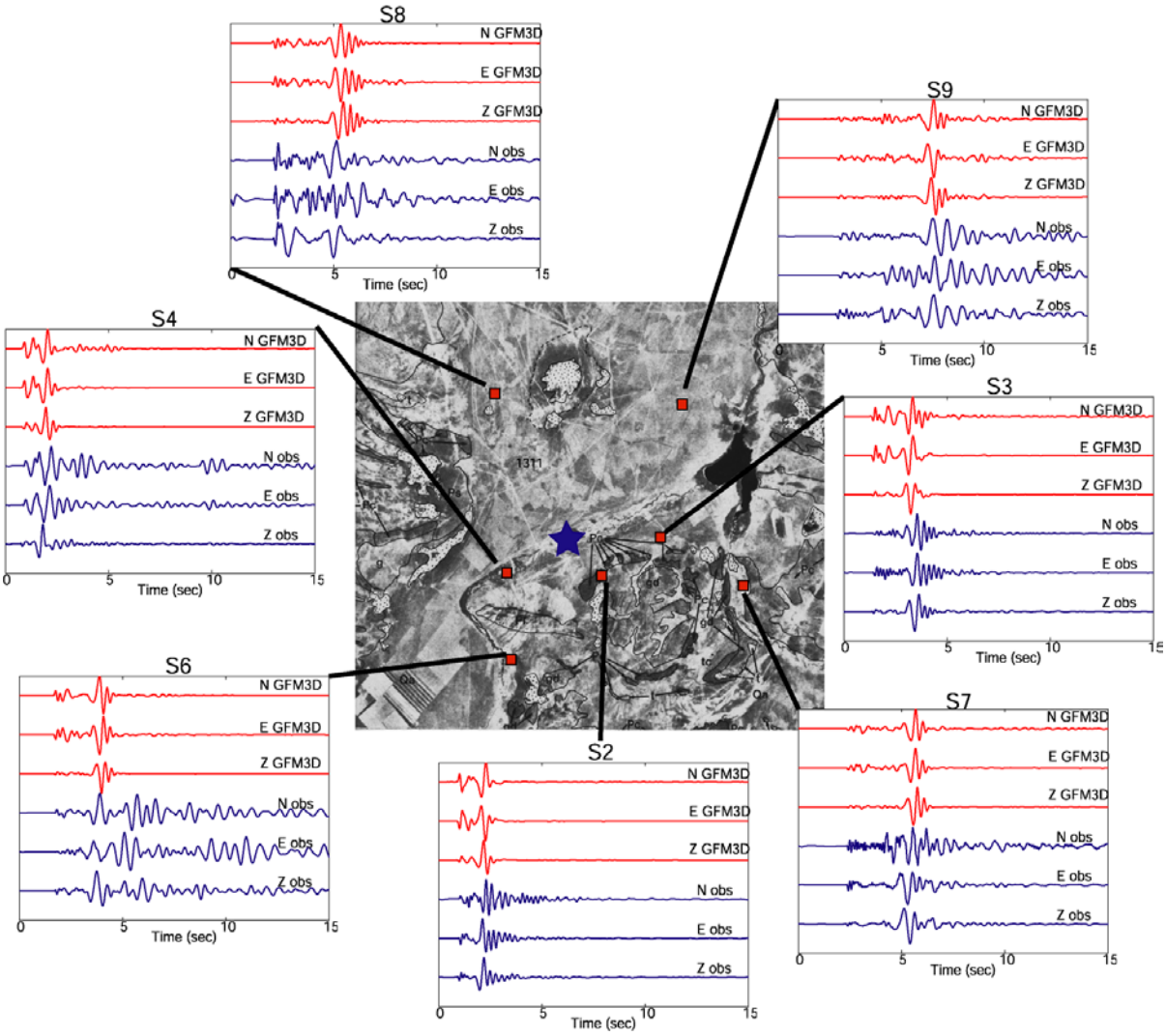

Figure 7. Comparison of observed local seismograms from the explosion at borehole 1381 with GFM3D synthetic traces. Each subplot corresponds to a station that recorded this 50-ton explosion at a depth of 300 m. The first three traces are the N, E, and Z traces synthesized using the STS velocity model and the GFM3D code followed by the observed N, E, and Z waveforms. All data were filtered between 0.5 and 4 Hz.

We had less success matching the waveforms at station S9 (Figure 6), which is located in the complex NE section of the STS. The observed data for this event shows the longest signal duration for the STS seismic network. One possible reason for the extended signal duration is reverberations in a near-surface low-velocity layer. The model in this region (Figures 2 and 3) does have a near-surface low-velocity layer. However, the relative amplitudes of these reverberations as compared to the data could not be matched. Also of interest at this station are the arrival times for *P*, *S*, and *Rg*. While the modeling predicts accurate arrival times for P and S (within 0.2 seconds of the observed data), the predicted *Rg* arrives 0.5 secs prior to the observed signal. As noted in Figure 3, the preliminary model in this complex region is essentially a 2D path with minimal 3D effects. It is possible that a more complex 3-D model in this region, possibly developed using borehole logs or laboratory *P*- and *S*-wave velocities from core samples, could improve the results for station S9.

We obtain similar success rates for modeling the explosion at 300 m depth in borehole 1381 (Figure 7). In these examples, we find a better fit to the S9 *P*, *S*, and *Rg* arrivals; however, we get poor matches with the data at stations S6 and S8. We also observe longer signal duration than modeled for the data at S6. Because of space limitations in

this paper, the results of the 550 m depth explosion at borehole 1349 are not presented but are available for review. These results, while preliminary, suggest the GFM3D method is an accurate technique to model the generation and propagation of short-period surface waves and body waves.

A second goal of the short-term modeling project at STS was to examine the addition of near-source random variations to the velocity values of the layered structure. In this regard, Figure 8 illustrates the effects of random spatial variations (max 10%) in the velocity values within 3 km of the source inside the STS model in both the vertical and lateral directions. Random variations in upper-crustal velocity structure measured in boreholes have often been found to be 25% and greater, thus a 10% fluctuation is not extreme and is probably conservative. We then modeled a point source explosion at 50 m depth and propagated the seismic energy to the stations shown in Figure 8. We then compared these data with random near-source heterogeneities to the GFM3D runs without the velocity variations (same data shown in Figure 6). The resulting seismograms and spectra for the modeling to station S7 are shown in Figure 9. The near-source scattering in the randomized model creates larger amplitudes for the entire *Rg* wave train; however, the most pronounced increase occurs in the 3 to 10 Hz frequency band. The increase in this frequency band may have very important ramifications in the generation of the regional distance *Lg* shear phase from explosions. In fact, Myers *et al.* (1999) examined the regional data from these explosions at STS and concluded that the dominant mechanism for enhanced regional *Lg* and *Sn* excitation for shallower 1311 explosion is local *Rg* scattering. Thus, to properly quantify the effect of this near source scattering at regional distances, we plan to develop a larger model for this region of Kazakhstan and model the regional seismograms for these explosions. We also plan to examine the effect of random variations along the entire path length in addition to the near-source regions.

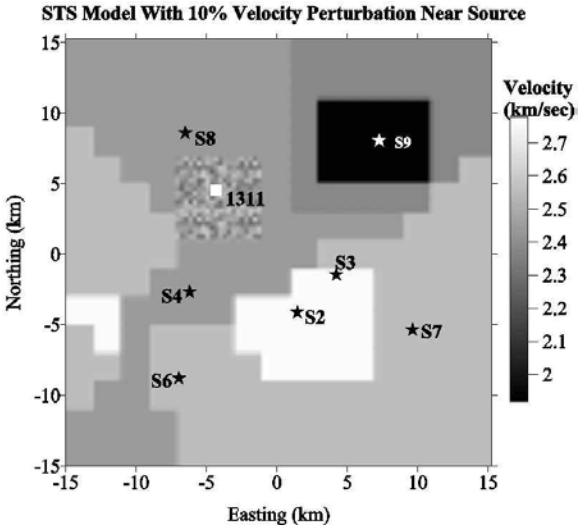

Figure 8. Shear-wave velocity at 0.2 km depth for a STS model with 10% near-soure velocity perturbations. Also shown are the location of borehole 1311 and stations that recorded this explosive borehole closure. The velocities have been randomized within 3 km of the source to examine the effects of near-source scattering on the *Rg* wave train.

CONCLUSIONS AND RECOMMENDATIONS

A parallelized version of the Generalized Fourier Method has been implemented on a nine-node Linux cluster system, and we have used the code to model the *Rg* generation and propagation from single-fired explosions at the former Soviet Union Test Site near the Shagan River (STS) in Balapan, Kazakhstan. The results using our initial 3D velocity models for STS are very encouraging and show the method is suitable to examine source characteristics such as radiation patterns and secondary effects (e.g. scattering). We will continue the modeling of these explosions at STS by refining the velocity models and by examining the effects of near-source scattering on regional data. In addition, we will incorporate our inferred Q models of the site into the GFM code, using the method of Emmerich and Korn (1987). Given the low inferred Q values in the NE section of the STS model, we expect the Q effects on the waveforms to be critical for an accurate characterization of the energy partitioning between body and surface wave phases. Also, we will work with David Yang of Los Alamos National Laboratory to combine his MineSeis1.1 (Yang, 1998) program with the GFM3D code. By combining realistic source effects from his code with the GFM3D wavefield synthesis, we expect to have a powerful and robust method for modeling the complexity of regional, explosion-generated surface waves propagated through various tectonic regimes.

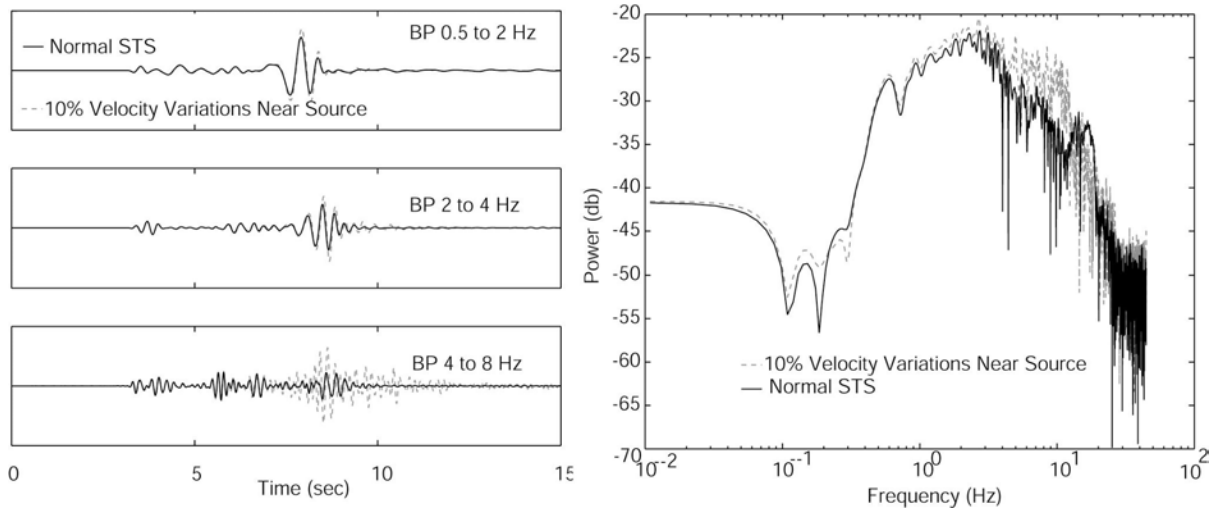

Figure 9. Seismograms and spectra for synthesized data at S7 showing the effects of applying 10% random velocity fluctuations to the near-source structure.

ACKNOWLEDGMENTS

We thank Howard Patton, David Yang, and Brian Stump for helpful comments on this research project. We also wish to thank D. Craig Pearson and Diane Baker for help acquiring the DOB data. Finally, we thank Delaine Reiter, Ileana Tibuleac, and Jim Lewkowicz for help with the manuscript and additional support with this project.

REFERENCES

Aki, K. and P.G. Richards (1980), Quantitative Seismology: Theory and Methods, W.H. Freeman, New York.

Bonner, J., D.C. Pearson, W.S. Phillips, and S.R. Taylor (2001), Shallow velocity structure of the Shagan River Test Site in eastern Kazakhstan, *Pure and Applied Geophysics,* 158, 2017-2039.

Davis, P. A., and G. L. Berlin (1992), Geologic mapping of the Semipalintisk region using Land Sat thematic mapper and spot panochromatic data, *LAUR-92-310*, 15 pp.

Emmerich, H. and M. Korn (1987), Incorporation of Attenuation into Time-Domain Computations of Seismic Wave fields, *Geophysics,* 52(9), 1252-1264.

Fornberg, B., (1987), The pseudospectral method: Comparisons with finite differences for the elastic wave equation, *Geophysics*, 52, 483—501.

Furumura, T., B. L. N. Kennett, and H. Takenaka (1998), Parallel 3-D pseudospectral simulation of seismic wave propagation, *Geophysics*, 63, 279—288.

Myers, S. C., W. R. Walter, K. M. Mayeda, and L. Glenn (1999), Observations in support of *Rg* scattering as a source for explosion S waves: regional and local recordings of the 1997 Kazakhstan depth of burial experiment, *Bull Seism. Soc. Am.*, 89, 544-549.

Orrey, J. L. and G. Robinson (2002), A Parallel Implementation of the Generalized Fourier Method for Elastic Wave Simulations, in preparation for submittal to *Geophysics*.

Orrey, J. L., C. B. Archambeau and G. A. Frazier (2002), Complete Seismic Wave Field Synthesis with a Pseudospectral Method: The Generalized Fourier Method, revised manuscript to be submitted to *Geophys. J. Int*.

Phillips, W.S., H. J. Patton, and H. E. Hartse (2001), Regional coda magnitudes in central Asia and $m_b(Lg)$ transportability, Proceedings *of the 23rd Annual Seismic Review: Worldwide Monitoring of Nuclear Explosions-October 2-5, 2001*, 580-589.

Ringdal, F., P. D. Marshall, and R. W. Alewine (1992), Seismic yield determination of Soviet underground nuclear explosions at the Shagan River test site, *Geophys. J. Int*. 109, 65-77.

Yang, X. (1998), MineSeis – A MATLAB GUI program to calculate synthetic seismograms from a linear, multi-shot blast source model, in *Proceedings of the 20th Annual Seismic Research Symposium on Monitoring a Comprehensive Test Ban Treaty*, 21-23 September, 1998, Santa Fe, New Mexico, 755-764.